Progress Report

ATMOSPHERIC INFRARED SOUNDER

NASA CONTRACT NAS5-31376

for the period

December 16, 1994 - June 15, 1995

Submitted to Team Leader
Moustafa T. Chahine
Jet Propulsion Laboratory
Pasadena, CA 91109

Submitted by

Team Members
Philip W. Rosenkranz
David H. Staelin

Research Laboratory of Electronics
Massachusetts Institute of Technology
Cambridge, MA 02139

August 22, 1995

1. Microwave first-guess algorithm

Changes to the microwave first-guess algorithm have separated processing of AMSU-A from AMSU-B data so that the different spatial resolutions of the two instruments may eventually be considered. However, at present only the center spot of the 3 x 3 AMSU-B cluster is being used in the moisture profile retrieval. AMSU-A data is used for retrieval of temperature profile and surface emissivity. The updated algorithm was delivered to JPL in May.

The two-layer cloud simulation data was processed with this algorithm. Figure 1 compares the retrieved water vapor column densities along the A track with the "true" data which was generated by the NMC eta model. Figure 2 shows the true and retrieved liquid water. Track A had surface emissivity of 0.9 in the simulation. The retrieval has difficulty with the heavy low cloud underlying dry air. Work on this algorithm is continuing.

2. Combined AIRS/AMSU retrievals

W.J. Blackwell has studied the information content of AIRS data as applied to temperature profile retrievals in clear and cloudy atmospheres. The TIGR profile ensemble was used for the simulation, and clouds were inserted wherever relative humidity exceeded 90%. In this simulation, clouds were considered to be opaque to IR and transparent to microwaves. Cloud coverage was uniformly distributed between 0% and 100%. Figure 3 shows the signal-to-noise ratio of clear-air AIRS channels in four groups, versus the eigenvalue number in a principal-component analysis. In each graph, the dashed curve is computed for averages of 9 AIRS measurements and the solid curve for 81 measurements. It is evident that reduction of noise by averaging substantially increases the number of degrees of freedom recoverable from the measurements. Figure 4 shows similar results for the cloudy case. The implication of this analysis is that it will be advantageous to use all of the AIRS channels rather than only a few, and to spatially smooth the measurements.

These conclusions were tested by a global linear retrieval in which the temperature profile $\underline{T}$ was estimated by a single matrix multiplication of the brightness temperature $\underline{T}_B$:

$$\underline{T} = \mathbf{D} \cdot \underline{T}_B.$$

The matrix D was different for land and sea surfaces. The land or sea emissivity was chosen by a neural network operation on AMSU channels 1,2,3,4, and 15. A rudimentary cloud-clearing of the IR channels was done by examining the average of 10 AIRS 15 μ-band channels that peak near 4-km altitude. The warmest of the 9 AIRS spots associated with an AMSU-A spot was used in the retrieval. Figure 5 compares retrievals with and without AMSU/MHS channels, showing the expected result that the microwave channels are necessary for good results in cloudy atmospheres. Figures 6 and 7 show retrieval results in clear and cloudy atmospheres, respectively, for two different spatial resolutions. It is seen that the reduction of noise by horizontal smoothing improves the retrieval accuracy in both cases, confirming the conclusions of the principal-component analysis.

The significance of this study for AIRS/AMSU processing lies in the improvement attributable to spatial averaging and in the good results obtained with a very simple algorithm when all of the channels are used. We recommend that the design of the operational algorithm should take advantage of (e.g. modify, then use) these concepts.

3. Alternatives to MHS

Uncertainty about the availability of either an MHS or AMSU-B for EOS has motivated consideration of possible low-cost alternative designs for a microwave humidity sounder. One possible configuration, discussed at the team meeting in February, would have two local oscillators (compared to three for MHS) at 118.75 and 183.31 GHz. Figures 8 and 9 plot weighting functions for this alternative instrument. The channel at 119 ± 6 GHz would substitute for the 89 GHz channel of MHS. The 119 ± 0.5 and 119 ± 1.4 GHz channels would provide information on altitude of clouds and rain not obtainable from MHS. C.R. Cabrera-Mercader and D.H. Staelin compared retrieval performances of the two instruments in a memorandum titled, "Comparative Analysis of Alternate MHS Configurations," which is attached.

Figure Captions

1. True (upper) and retrieved (lower) cross-section of water vapor (g/cm^2 in 25-mb layers) between 400 and 1,000 mb along track A.

2. True and retrieved liquid water, as in Fig. 1.

3. Principal-component analysis of AIRS channels in four groups, for clear air.

4. As in Fig. 3 , for cloudy air.

5. Temperature retrieval errors in cloudy air using AIRS/AMSU-A/MHS (left curve) and AIRS only (right curve).

6. Temperature retrieval errors in cloudy air using AIRS/AMSU-A/MHS at 45-km resolution (solid line) and 135-km resolution (dashed line).

7. As in Fig. 6, for clear air.

8. Weighting functions for an MHS-alternative at vertical incidence.

9. Weighting functions as in Fig. 8, for 60° from vertical.

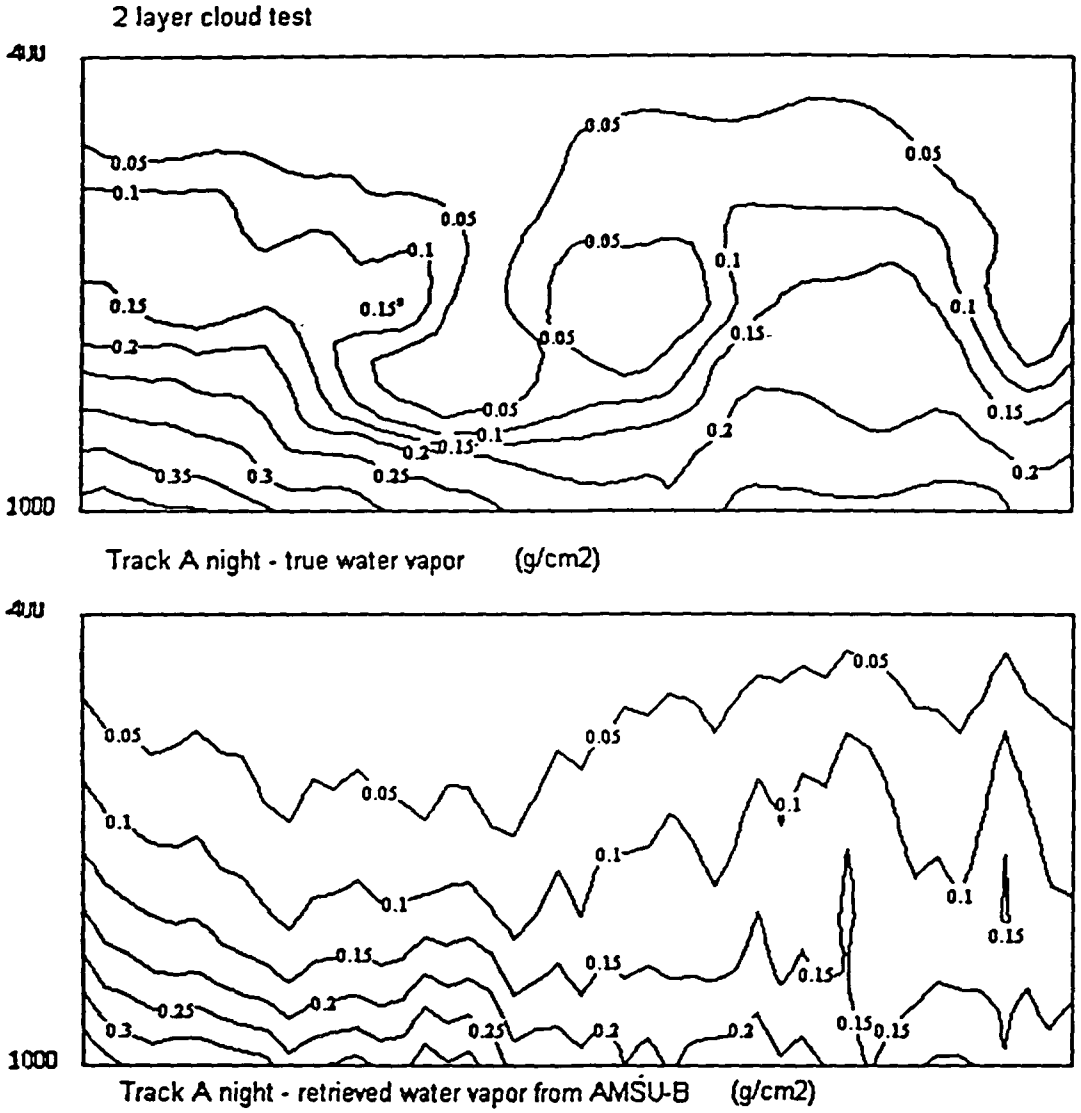
2 layer cloud test
400
1000
Track A night - true water vapor (g/cm2)
400
1000
Track A night - retrieved water vapor from AMSU-B (g/cm2)

Figure 1

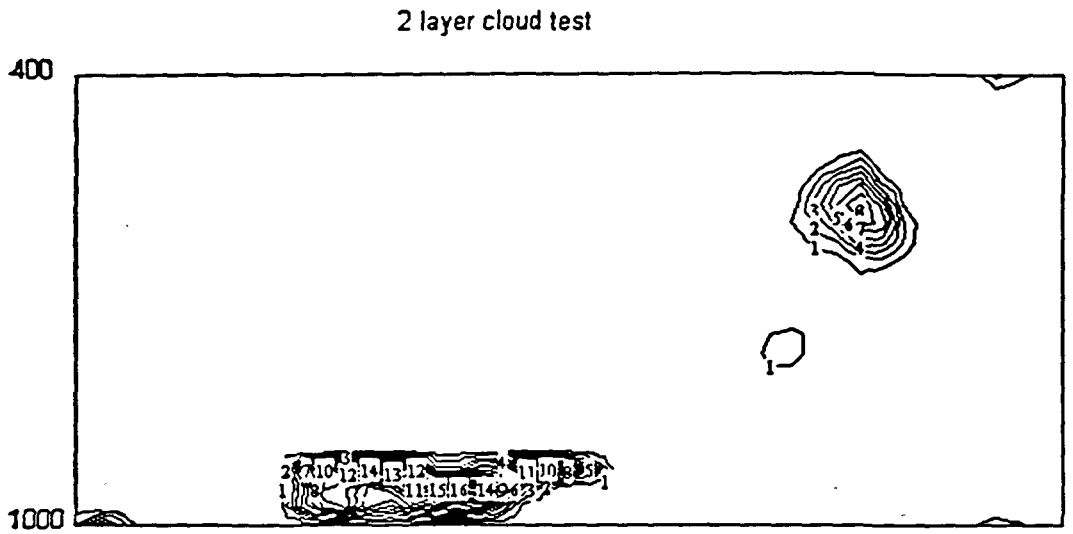

Track A night - true liquid water (mg/cm2)

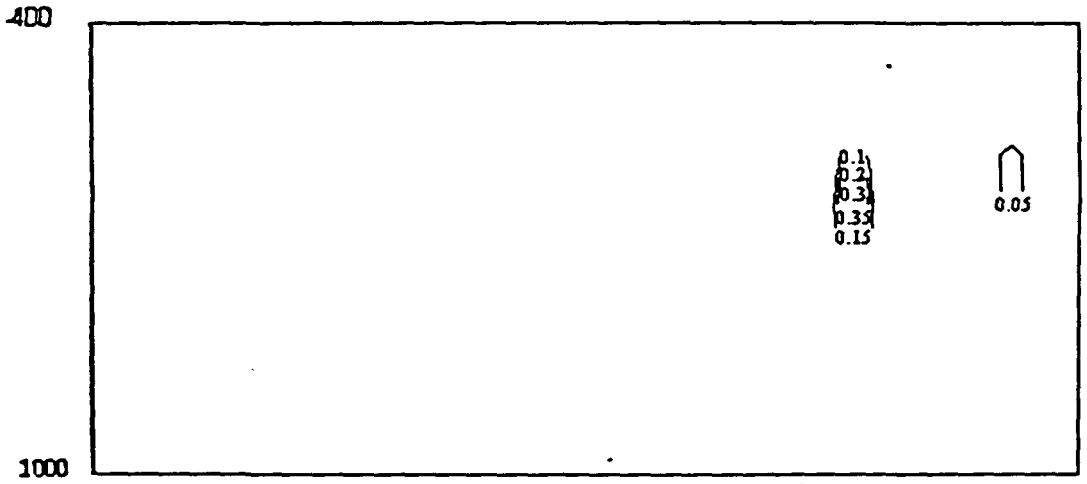

Track A night - retrieved liquid water from AMSU-B (mg/cm2)

Figure 2

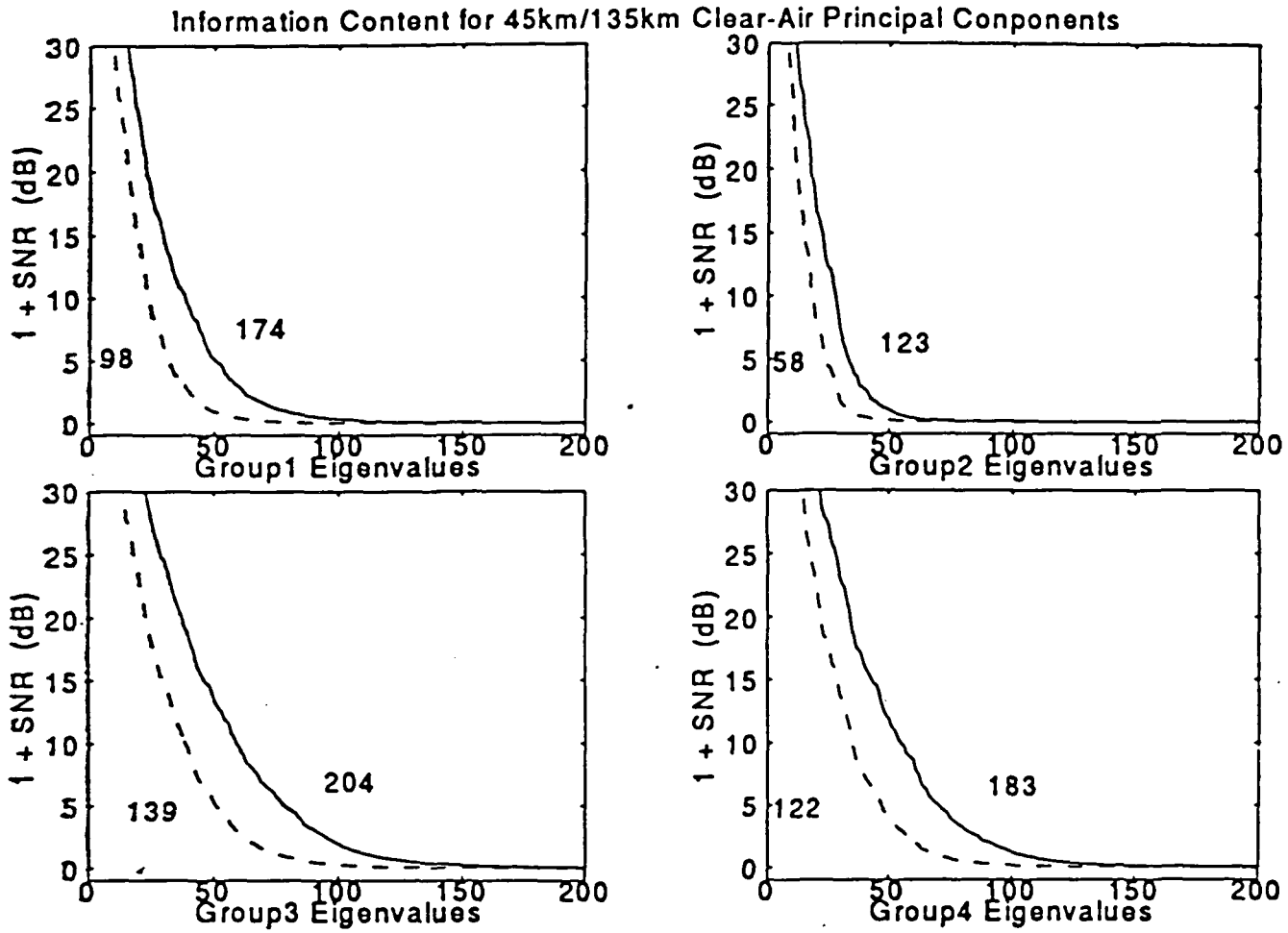

SNR IS $\frac{\text{NOISE-FREE VARIANCE OF EIGENVECTORS}}{\text{VARIANCE DUE TO RECEIVER NOISE}}$

AIRS	1.	15-MICRON BAND	(CH. 1-593)
CHANNEL	2.	WINDOW CHANNELS	(CH. 594-1186)
GROUP	3.	WATER VAPOR BAND	(CH. 1187-1779)
	4.	4-MICRON BAND	(CH. 1780-2371)

- - - - - 45-KM RESOLUTION (9-SPOT AVERAGE)
_____ 135-KM RESOLUTION (81-SPOT AVERAGE)

Figure 3

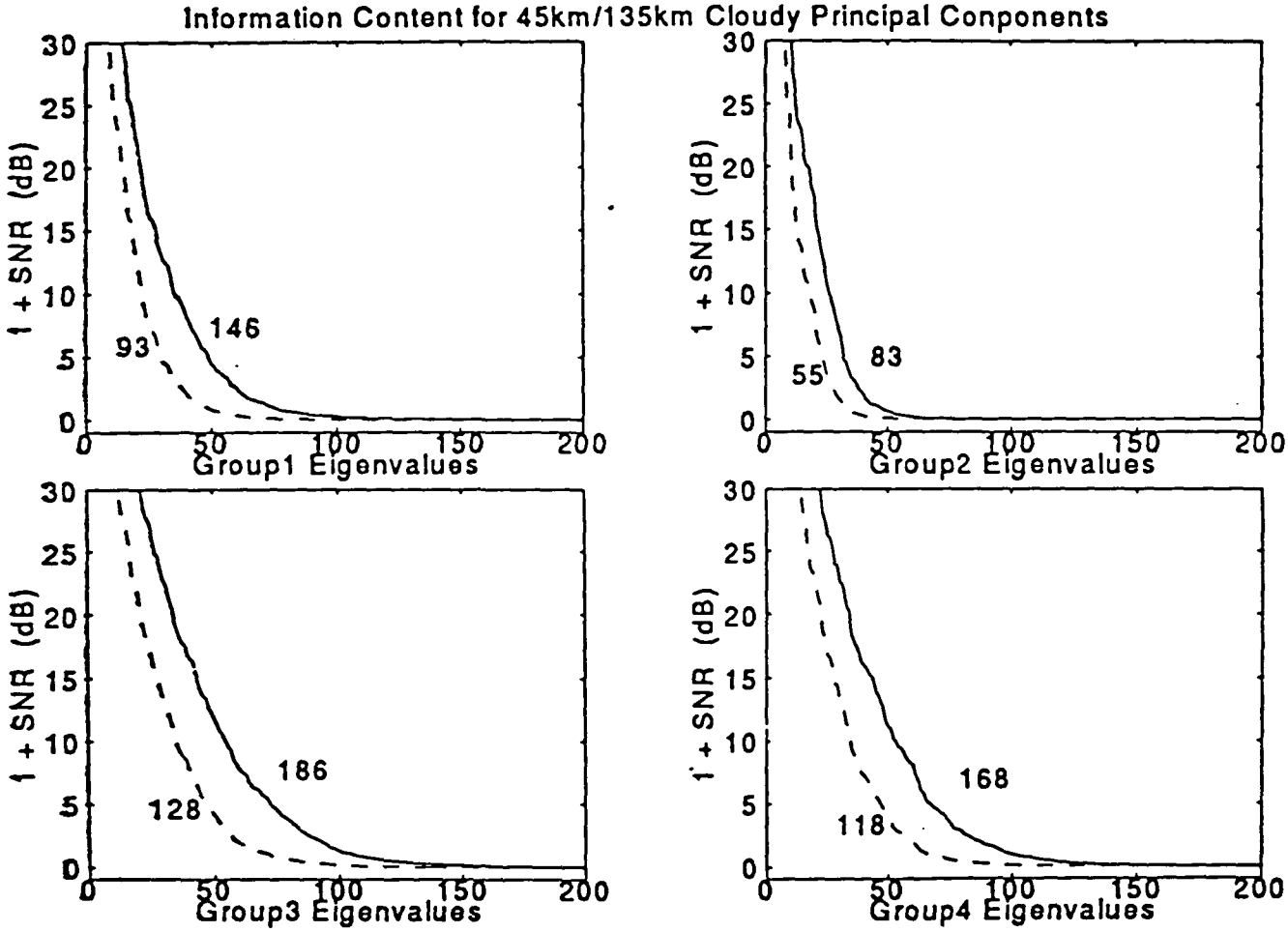
Information Content for 45km/135km Cloudy Principal Conponents
1 + SNR (dB)
Group1 Eigenvalues
93
146
Group2 Eigenvalues
55
83
Group3 Eigenvalues
128
186
Group4 Eigenvalues
118
168

Figure 4

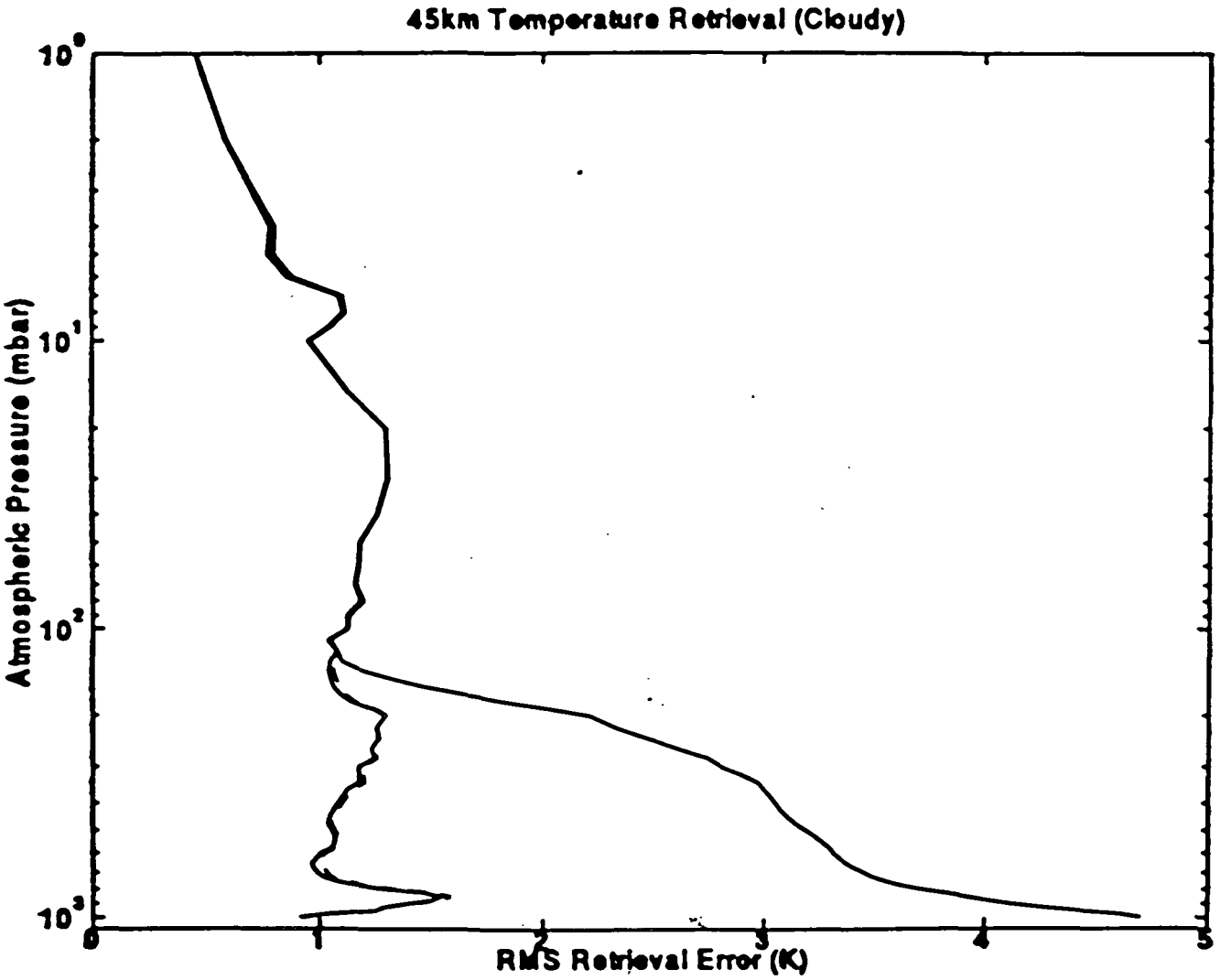
45km Temperature Retrieval (Cloudy)
Atmospheric Pressure (mbar)
10^0
10^1
10^2
10^3
0
1
2
3
4
5
RMS Retrieval Error (K)

Figure 5

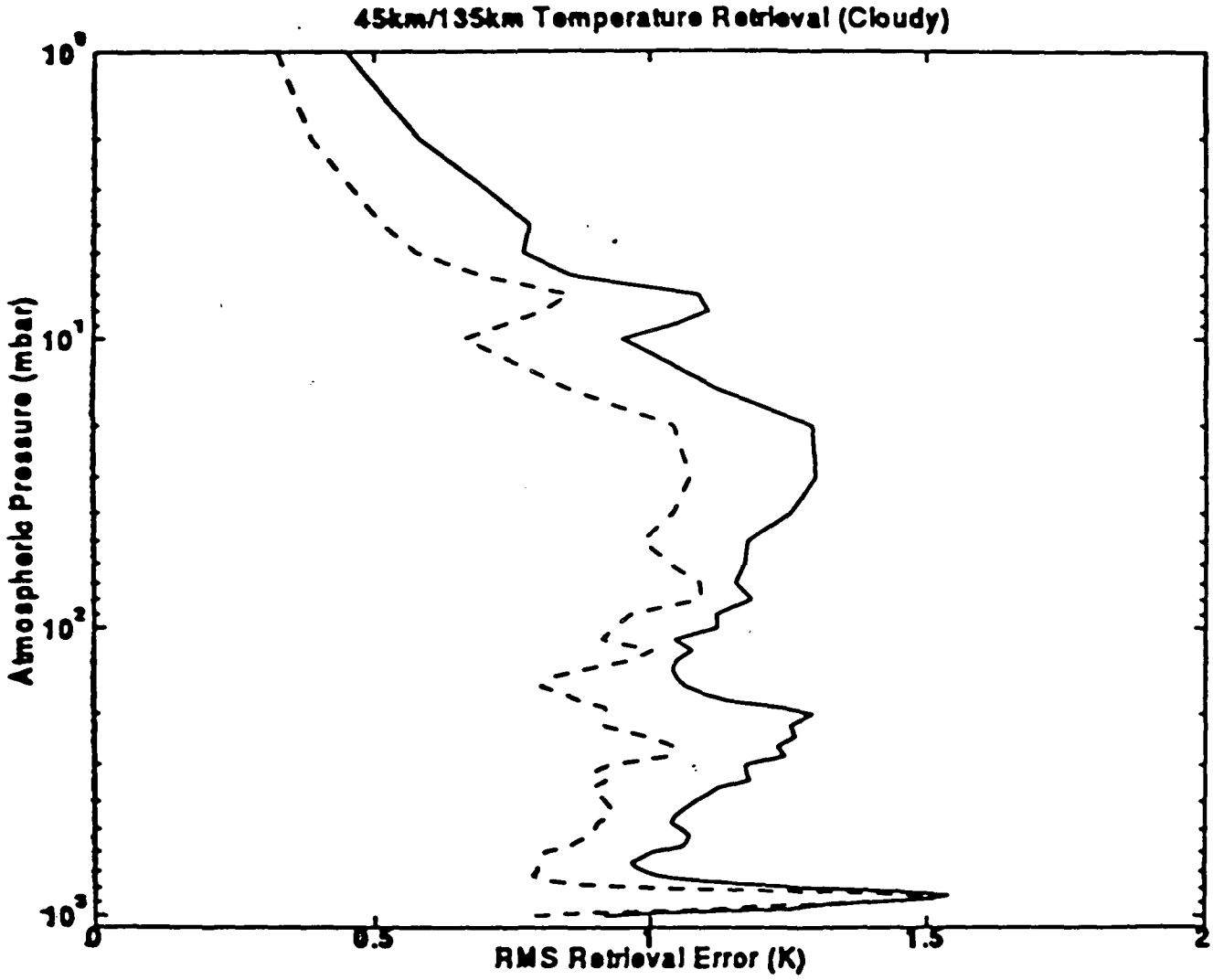
45km/135km Temperature Retrieval (Cloudy)
Atmospheric Pressure (mbar)
10^0
10^1
10^2
10^3
0
0.5
1.5
2
RMS Retrieval Error (K)

Figure 6

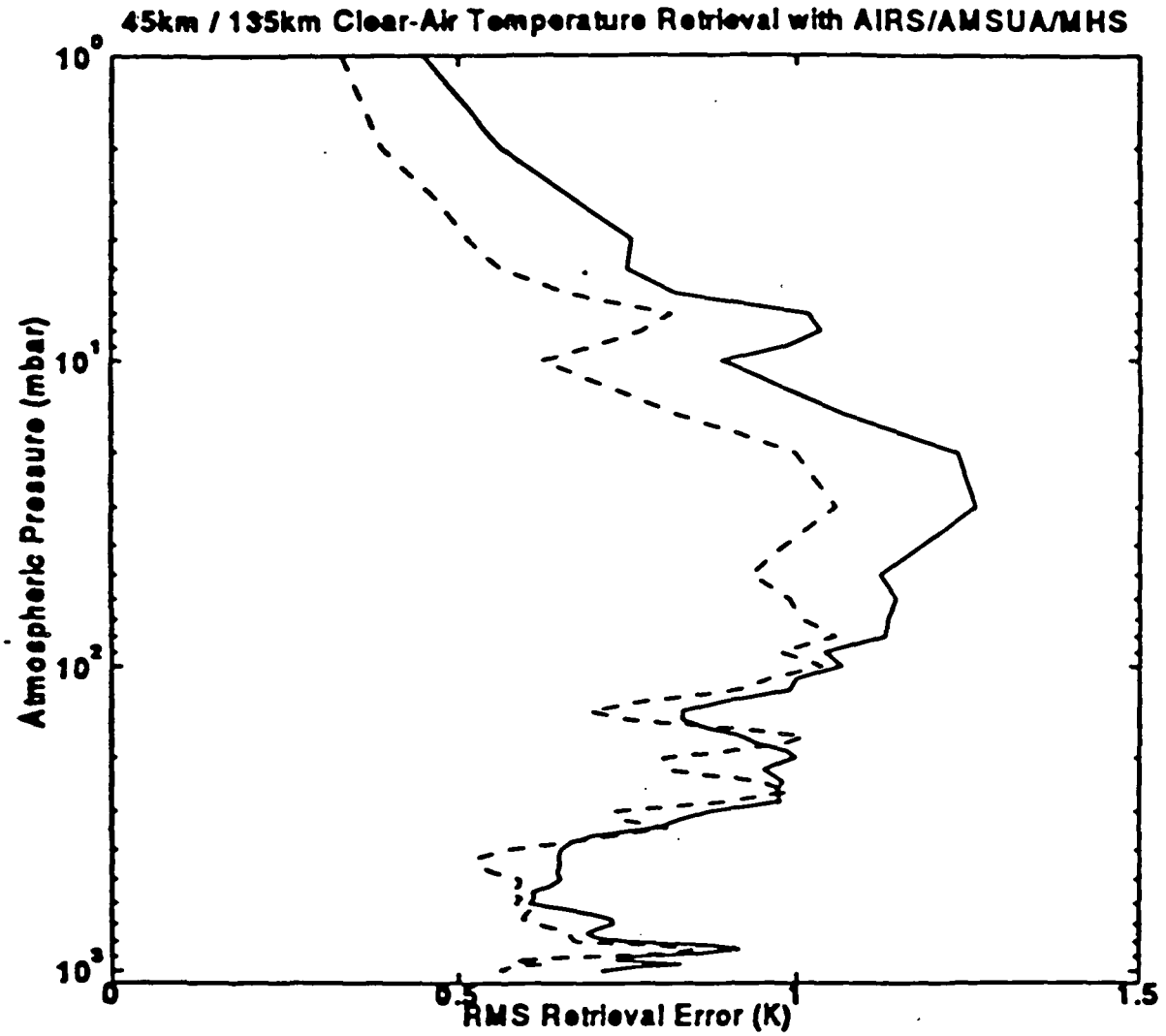
45km / 135km Clear-Air Temperature Retrieval with AIRS/AMSUA/MHS
Atmospheric Pressure (mbar)
10^0
10^1
10^2
10^3
0
0.5
1
1.5
RMS Retrieval Error (K)

Figure 7

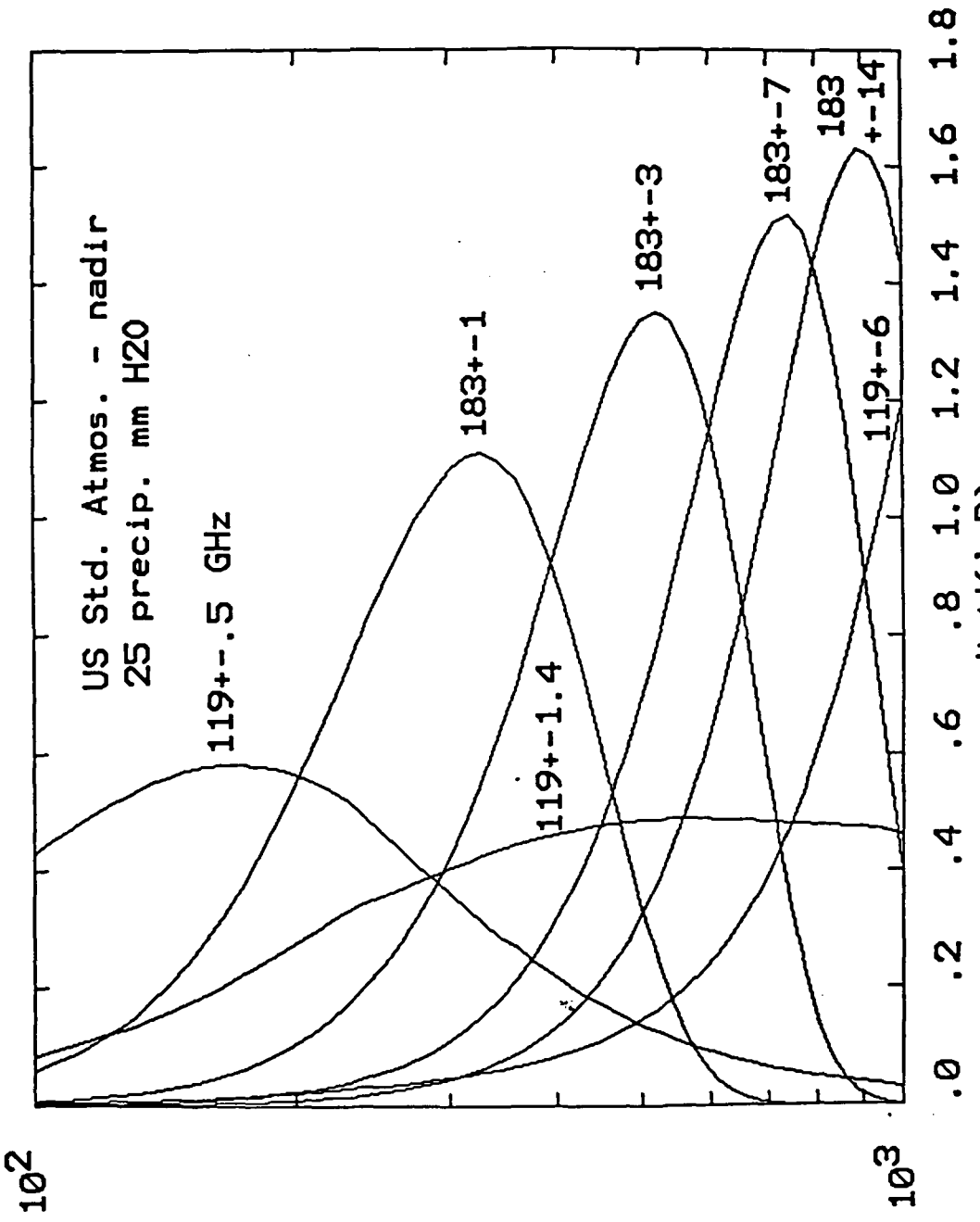
US Std. Atmos. - nadir
25 precip. mm H20
119+-.5 GHz
183+-1
119+-1.4
183+-3
183+-7
183 +-14
119+-6
PRESSURE (mb)
10^2
10^3
.0 .2 .4 .6 .8 1.0 1.2 1.4 1.6 1.8
dt/d(lnP)

Figure 8

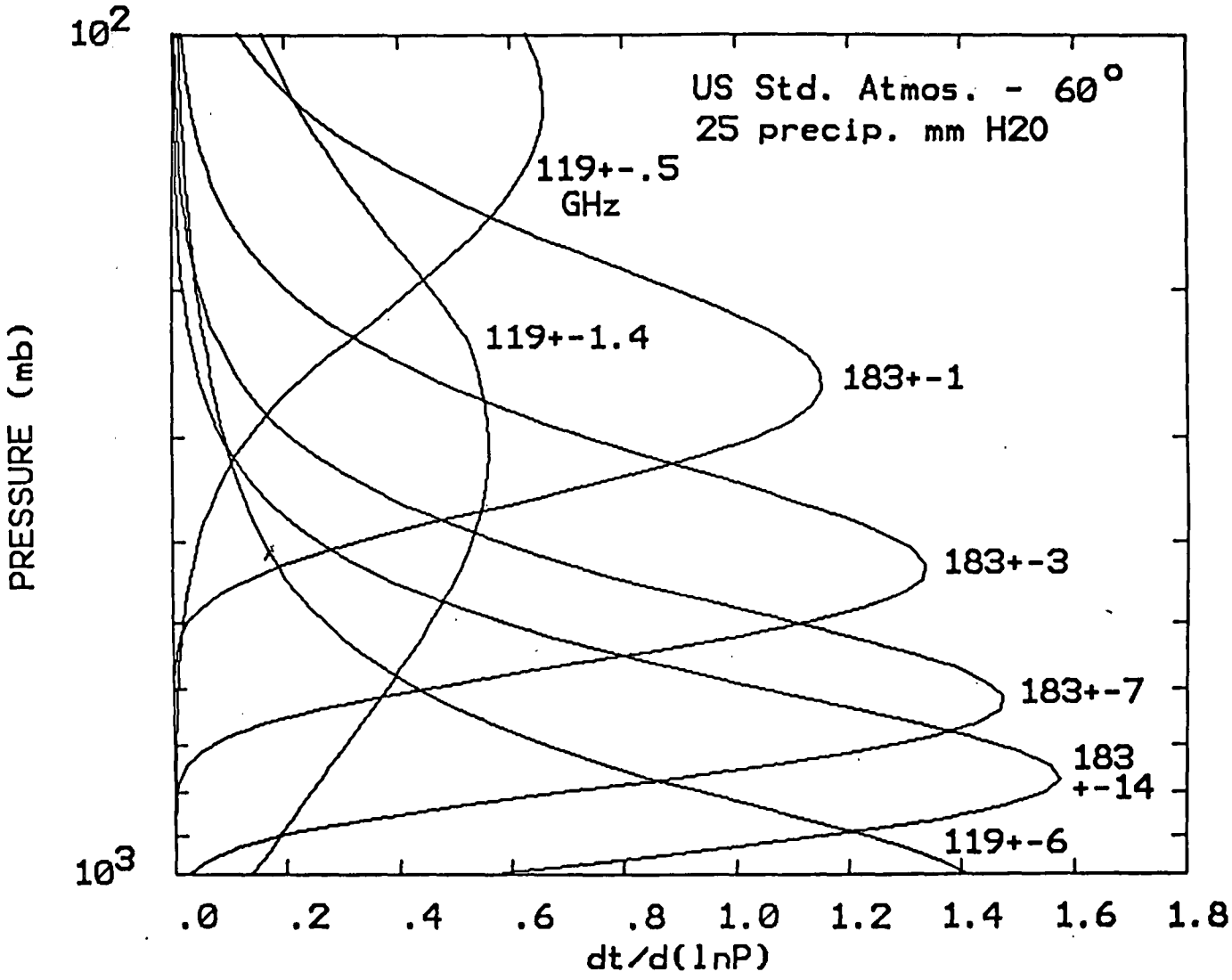
US Std. Atmos. - 60°
25 precip. mm H20
119+-.5
GHz
119+-1.4
183+-1
183+-3
183+-7
183
+-14
119+-6
PRESSURE (mb)
10^2
10^3
.0
.2
.4
.6
.8
1.0
1.2
1.4
1.6
1.8
dt/d(lnP)

Figure 9

Comparative Analysis of Alternate MHS Configurations

Carlos R. Cabrera-Mercader
David H. Staelin
Massachusetts Institute of Technology

June 29, 1995

Executive Summary

Given the possibility that the passive Microwave Humidity Sounder (MHS) for NASA's Earth Observing System (EOS) may have to be replaced, two alternate configurations are analyzed in this document. One option mirrors AMSU-B, the Advanced Microwave Sounding Unit (AMSU) moisture sounder; which consists of five channels at 89, 150, 183 ± 1, 183 ± 3, and 183 ± 7 GHz. The second option contains an additional channel at 183 ± 14 GHz and replaces the channels at 89 and 150 GHz with three channels at 118 ± 0.5, 118 ± 1.4, and 118 ± 3 GHz. The latter configuration is considered to be superior due to its greater scientific benefits and reduced cost and complexity – it would require only two local oscillators and a smaller antenna size for a given resolution on the ground. As shown by means of simulations, humidity profile retrieval accuracy for the second option is superior in most cases and only slightly degraded relative to the first option in the worst-case scenario. The results are summarized in Appendix C. Including the 118-GHz channels also offers the possibility of cell-top altitude retrievals and improved temperature profile retrievals when used in conjunction with a temperature sounder such as the 15-channel AMSU-A.

1. Introduction

The Microwave Humidity Sounder (MHS), a five-channel microwave radiometer with channels centered at 89, 157, 183 ± 1, 183 ± 3, and 183 + 7 GHz, is one of the instruments planned to fly aboard the EOS-PM satellites. Along with the Advanced Microwave Sounding Unit (AMSU-A) temperature sounder and the Atmospheric Infrared Sounder (AIRS), MHS will be useful in measuring atmospheric water vapor profiles. Given that the availability of MHS is uncertain, two alternate configurations are analyzed in this document. We focus on humidity profile retrieval accuracy using the MHS substitutes alone and in combination with AMSU-A channels.

2. Specification of Alternate MHS Configurations

The channels of the MHS configurations being considered are drawn from the set of channels displayed in Table 1. The first option has the same channels as AMSU-B, these are channels one through five. We will refer to this option as MHS5. The second option consists of channels three to nine and will be referred to as MHS7.

No.	Center Freq. (GHz)	RMS Sensitivity (K)	MHS5	MHS7
1	89.0	0.8	√	
2	150.0	0.8	√	
3	183.31 ± 1.0	0.8	√	√
4	183.31 ± 3.0	0.8	√	√
5	183.31 ± 7.0	0.8	√	√
6	183.31 ± 14.0	0.8		√
7	118.75 ± 0.5	0.8		√
8	118.75 ± 1.4	1.0		√
9	118.75 ± 3.0	0.8		√

Table 1: Channels being considered for the MHS instrument.

3. Simulated Relative Humidity Profile Retrievals

3..1 Retrieval Method

The retrieval method used here is a global statistical inversion approach using multilayer feed-forward neural networks. The inversion is "direct" in the sense that a network is used to map the space of brightness spectra to the space of humidity profiles so as to minimize a cost function. In our case the networks were trained by error backpropagation to minimize the sum of squared errors in the retrieved profiles evaluated on a set of data.

For a description of multilayer neural networks and the backpropagation algorithm please refer to Rumelhart *et al.* [Rum86].

Retrievals were simulated over land and ocean, at nadir and fifty degrees incidence angle (measured with respect to the normal to the surface), under clear and cloudy conditions, and using MHS only or in conjunction with AMSU-A channels. For each separate case and each of the MHS configurations, a neural network was trained to perform retrievals of relative humidity profiles from simulated radiances. All the networks had an input layer of appropriate size to accomodate the desired number of channels, two hidden layers of nonlinear (sigmoid) units, and an output layer of twenty linear units, each of them giving an estimate of relative humidity at a particular pressure level. The number of hidden units was chosen based on previous experience and ranged from fifteen to thirty-six in the first hidden layer (the one following the input layer), and from five to eighteen in the second hidden layer.

The networks were trained and tested using two data sets consisting of 1,361 and 400 spectrum-radiosonde pairs, respectively. The atmospheric data was obtained from the TIGR (Thermodynamic Initial Guess Retrieval) radiosonde database [Esc93]. As shown in Tables 2 and 3 these soundings were made througout the calendar year, predominantly at the midlatitudes; a large number of them during the months of January and February. The training and validation data sets were completed with brightness spectra computed from these radiosondes (See Appendix A). The training data were actively used to adjust the parameters of the network so that the retrieval errors evaluated on these data were progressively reduced. The retrieval error evaluated on the validation data set was also monitored during training to detect and preclude any significant overfitting of the training data. Overfitting was also partly prevented by adding different noise samples to the brightness spectra during each training epoch as opposed to using a fixed ensemble of noise samples during the whole training phase.

Details regarding the computation of radiances and the cloud model can be found in Appendices A and B, respectively.

3..2 Retrieval Accuracy

A comparison of the proposed MHS configurations in terms of humidity profile retrieval accuracy is presented in this section. The retrieval method used here employs multilayer neural networks as described in the previous section. All the results presented in this section are root-mean-square retrieval errors evaluated on a validation data set of 400 spectrum-radiosonde pairs. For a summary of these results refer to Appendix C.

Figures 1 and 2 show the residuals over ocean under clear and cloudy conditions, respectively, using MHS5 and MHS7. Retrieval errors at both nadir and 50° incidence angle are included in the figures. In the lower troposphere (below $\sim$ 8 km) the errors are comparable in all cases. With clear-sky radiances the errors are mostly below fifteen percent of saturation using MHS7, and up to two percent higher with MHS5. In the same range

	−80°	−60°	−40°	−20°	0°	20°	40°	60°	80°
Jan	2	12	21	15	6	11	30	65	25
Feb	1	11	11	4	5	24	42	145	87
Mar	5	11	6	1	0	2	16	37	26
Apr	3	18	7	4	2	1	6	19	24
May	5	30	9	4	4	7	2	9	11
Jun	4	32	20	8	3	1	9	5	12
Jul	0	25	15	9	1	0	7	12	9
Aug	1	31	14	4	2	1	4	9	5
Sep	6	51	4	5	3	0	1	5	5
Oct	7	67	20	5	1	2	2	6	3
Nov	16	62	3	5	1	0	3	0	0
Dec	4	12	6	2	2	3	7	12	1

Table 2: Distribution by month and latitude of the radiosondes in the training data set. Numbers higher than or equal to thirty are in boldface.

	−80°	−60°	−40°	−20°	0°	20°	40°	60°	80°
Jan	0	11	6	8	1	2	8	14	7
Feb	1	2	3	2	1	10	15	32	27
Mar	1	1	2	0	0	4	3	9	9
Apr	2	2	2	1	0	0	1	5	3
May	1	8	3	1	0	0	0	0	4
Jun	3	11	5	4	0	0	1	2	5
Jul	0	6	3	2	0	0	1	1	3
Aug	0	18	0	0	0	0	0	0	2
Sep	2	18	5	2	1	0	1	2	2
Oct	1	26	8	3	1	1	2	0	1
Nov	5	15	2	3	0	0	1	0	0
Dec	0	5	1	1	0	2	4	6	0

Table 3: Distribution by month and latitude of the radiosondes in the validation data set. Numbers higher than or equal to ten are in boldface.

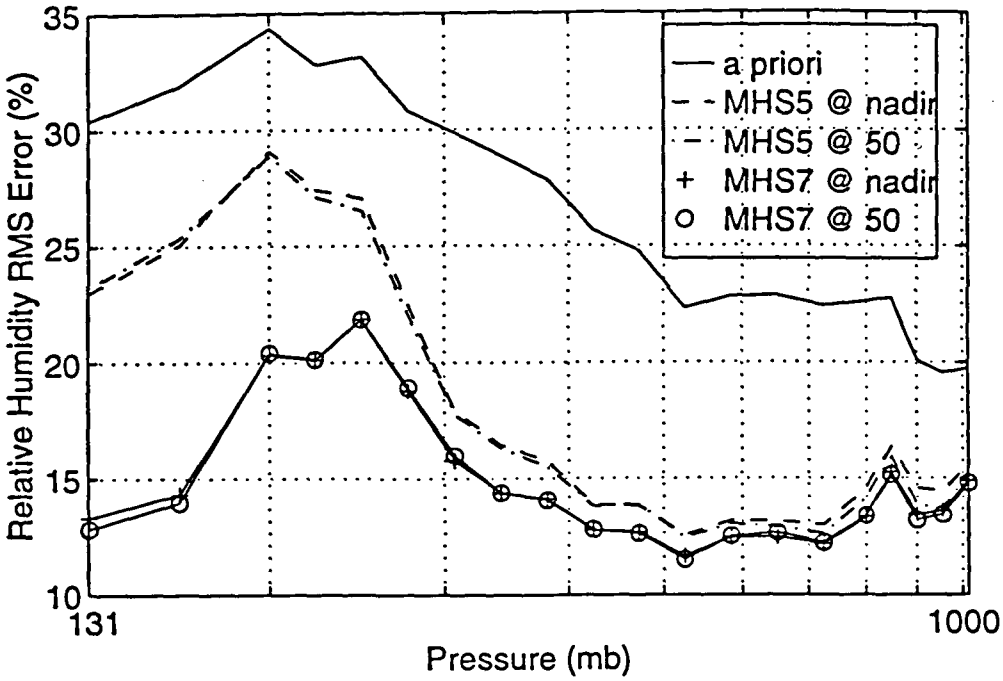

Figure 1: Comparison of clear-air retrieval accuracy over ocean.

of altitudes, retrievals from cloud-contaminated radiances yielded residuals mostly above fifteen percent of saturation using MHS7 and less than two percent higher using MHS5. The retrieval errors peak around 200 mb and, in the case of clear-sky radiances from MHS5, are very close to the a priori uncertainty.

While the retrieval accuracy in the lower atmosphere deteriorated with the addition of clouds, the opposite occured at higher altitudes. The improvement at higher altitudes is because, in our model, the presence of a cloud at a given altitude is perfectly correlated with a high relative humidity ($\geq$ 90%) at that altitude. Around 200 to 300 mb, the atmosphere is quite cold and can not hold much water vapor, thus the absorption at frequencies near 183 GHz is not significant. If a cloud is present, however, the absorption at these frequencies can increase substantially due to cloud liquid water, thereby giving strong evidence of the presence of water vapor. Thus, in the upper troposphere the retrieval is mostly statistical in nature. Clouds in this part of the atmosphere affect the retrieval adversely at low altitudes because the increase in absorption tends to move the weighting functions to higher altitudes.

The residuals shown in Figure 2 correspond to a validation data set of 400 radiosondes, of which roughly half had clouds added. Thus the actual retrieval degradation for cloudy atmospheres, i.e. the increment in retrieval error due to the addition of clouds, is slightly higher than shown there. Figure 3 shows the degradation for the cloudy atmospheres exclusively.

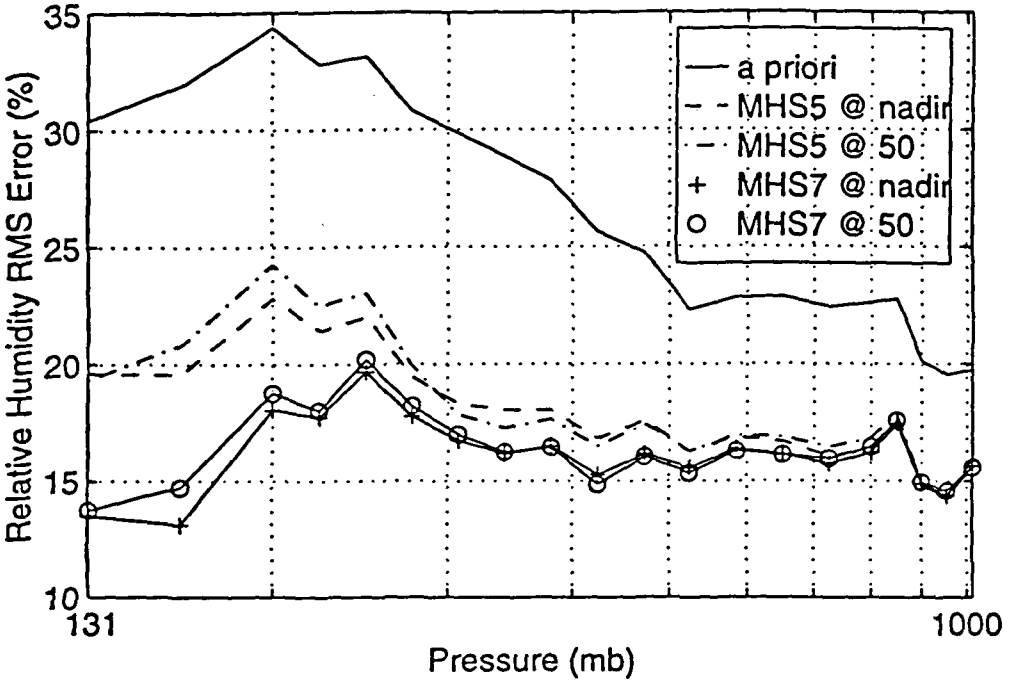

Figure 2: Comparison of cloudy retrieval accuracy over ocean.

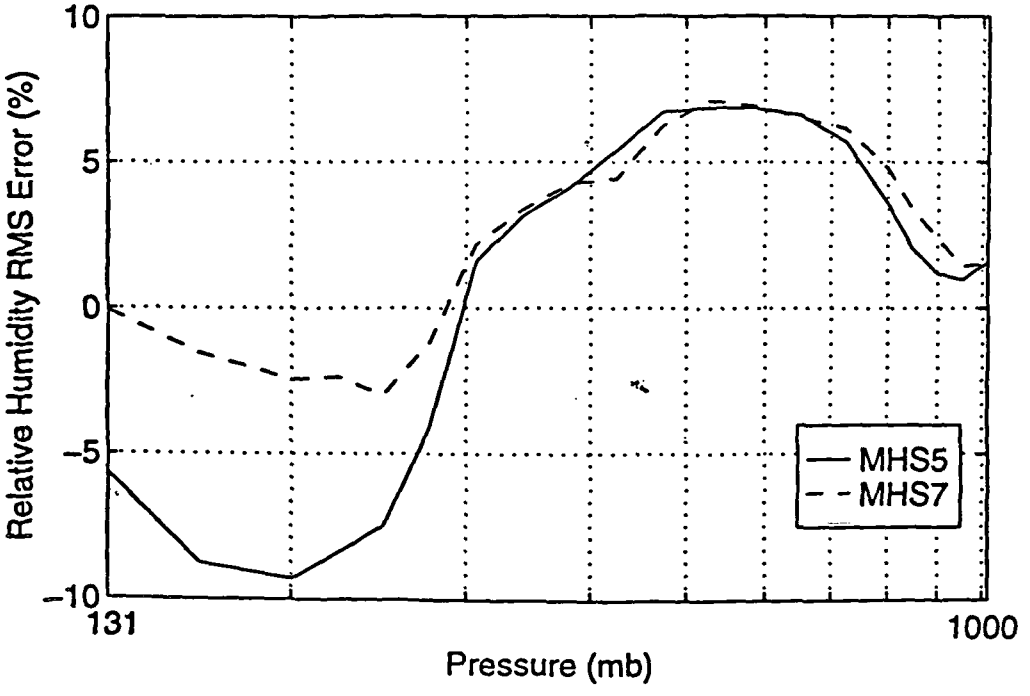

Figure 3: Degradation due to clouds of the retrieval accuracy over ocean.

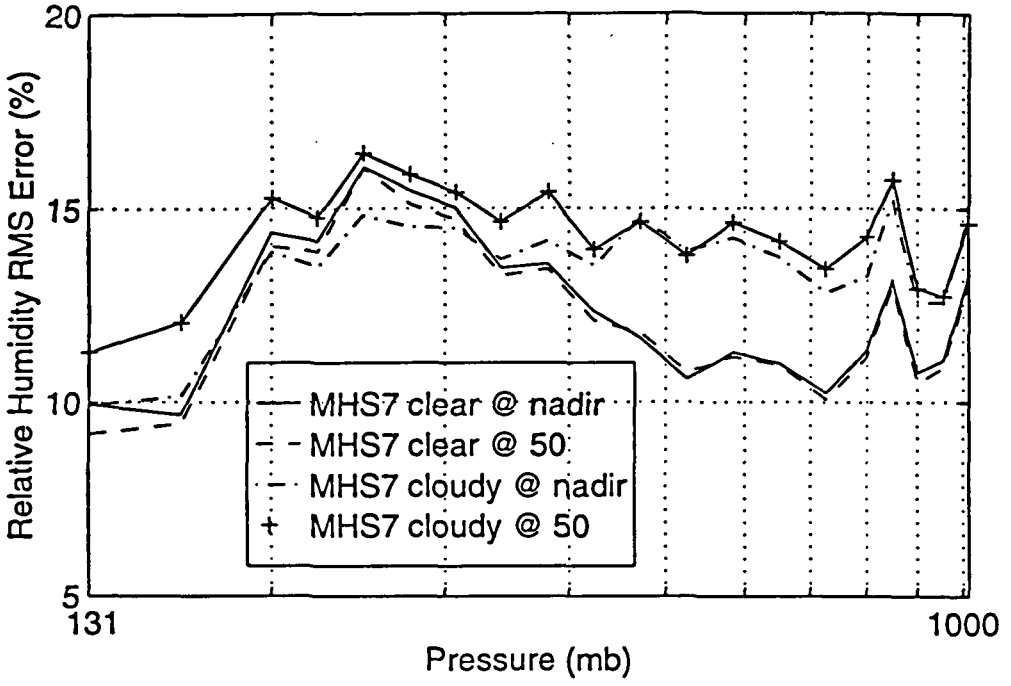

Figure 4: Retrieval accuracy over ocean of MHS7 combined with AMSU-A.

The accuracy of combined retrievals over ocean with AMSU-A is substantially better for both configurations. In Figure 4 are shown residuals of combined retrievals using MHS7 and AMSU-A. These results represent improvements over those for MHS7 alone of one to three percent of saturation at the lower levels (up to 300 mb), and of three to six percent at higher altitudes. Clouds affect the retrieval mostly at low altitudes, causing the errors to increase by up to three percent. The corresponding results for MHS5 are very similar. Figure 5 shows that the retrieval errors for both configurations differ by less than one percent of saturation in all cases.

Over land one expects the retrievals to be less accurate in the lower atmosphere due to stronger emission by the surface. Retrieval errors in the worst-case scenario, at 50° incidence angle over cloudy skies, are shown in Figure 6 for both MHS5 and MHS7. Comparing these results with those shown in Figure 2 the errors have increased by up to 3 percent at low altitudes. However, at altitudes above 500 mb ($\sim$ 5 km) the errors over land and over ocean are virtually identical. As Figure 6 indicates, MHS7 produces lower retrieval errors than MHS5 at high altitudes. This is likely due to a better ability to sense temperature provided by the 118-GHz channels.

The best-case scenario over land would be a combined retrieval with AMSU-A looking at nadir over clear skies. Simulations showed that in this case the retrieval errors are almost identical using both MHS configurations. The resuts are tabulated in Appendix C.

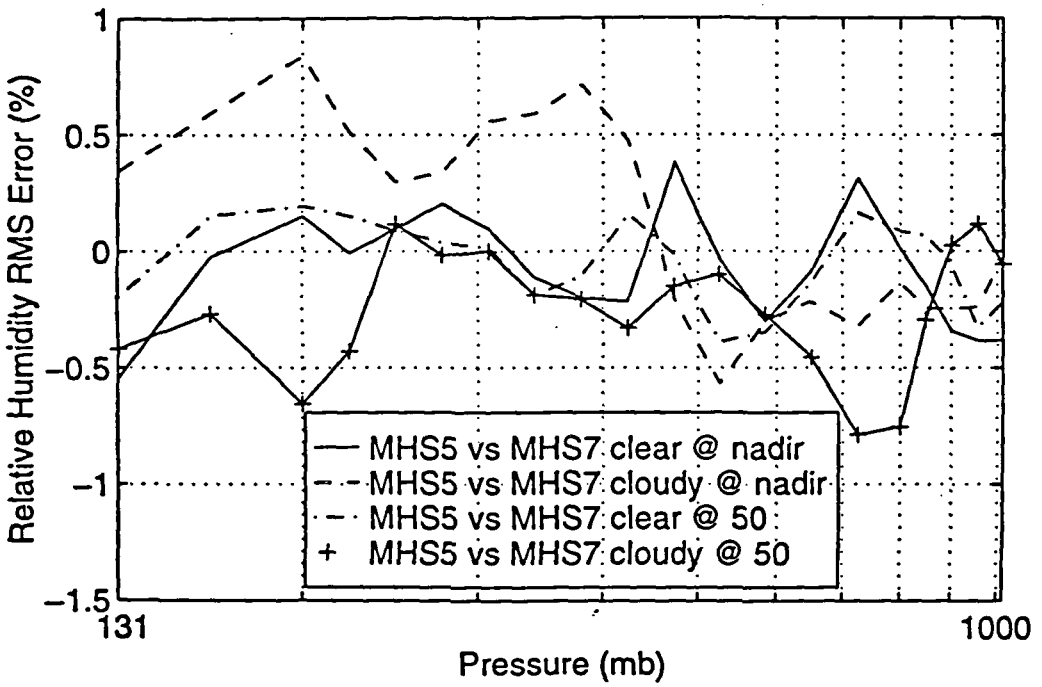

Figure 5: Comparison of retrieval accuracy over ocean using each of the MHS alternatives combined with AMSU-A. In each case the retrieval error using MHS5 minus the error using MHS7 is shown.

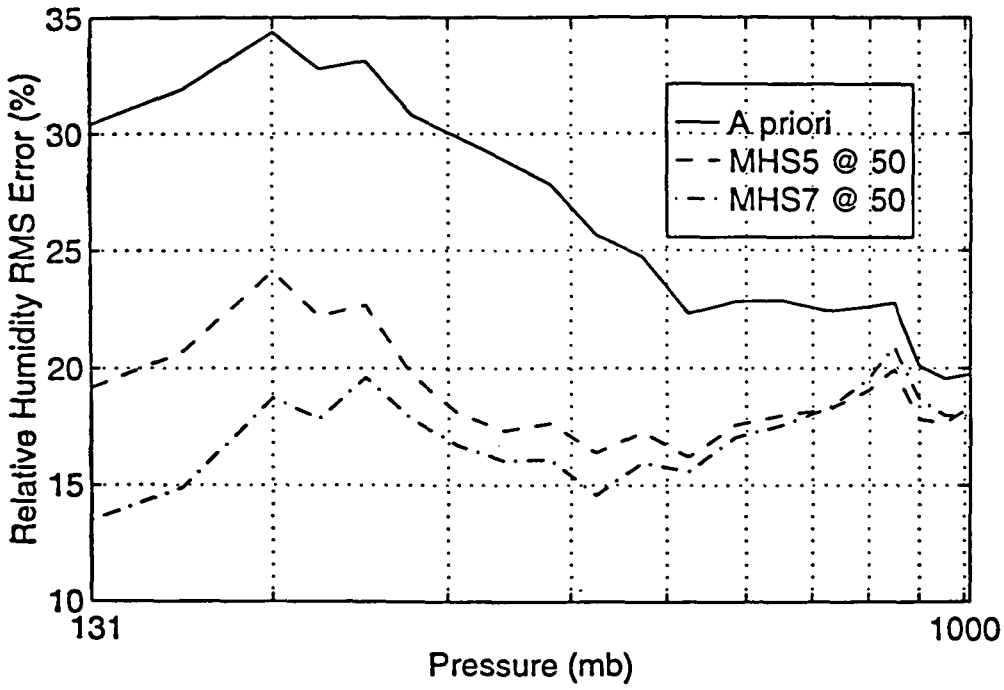

Figure 6: Comparison of cloudy retrieval accuracy over land at 50° incidence angle.

4. Conclusion

We have compared two alternate configurations of the MHS instrument in terms of the accuracy of simulated humidity retrievals. The results presented here indicate that when MHS is used alone in order to achieve full fifteen-kilometer resolution,then the MHS7 option, which includes four channels near 183 GHz and three channels near 118 GHz, is superior to MHS5, a five-channel configuration very similar to the original MHS specification. Global relative humidity retrievals from 131 mb to 1000 mb obtained with MHS7 were in general more accurate than those obtained with MHS5. Only close to the surface, in some cases, were the retrievals obtained using MHS5 were slightly better. When AMSU-A data is combined with MHS data, the two MHS configurations are more nearly comparable, with the rms difference being less than one percent relative humidity.

The good accuracy of humidity retrievals, the reduced cost of the system, and, in addition, the possibility of cell-top altitude retrievals and improved temperature retrievals offered by the addition of the 118-GHz channels, make the MHS7 configuration an attractive alternative to consider if a replacement to MHS is needed.

A Simulation of Radiances

The retrievals presented in the previous sections made use of synthetic microwave spectra derived for the TIGR radiosonde database. The original forty-level version of TIGR contains both temperature and water vapor profiles, and surface temperature in each of 1,761 radiosondes. These data along with assumed surface properties were input to a discretized non-scattering atmospheric radiative transfer model to produce brightness spectra. Relevant details of the computation of brightness temperatures are discussed below.

Two modifications of the TIGR data were necessary before radiances were computed. Several of the water vapor profiles were supersaturated according to our relative humidity calculation, which assumed saturation over ice at temperatures below 233.16 Kelvin and saturation over liquid otherwise. These profiles were modified so that saturation was not exceeded at any altitude. Finally, the surface temperature of the radiosondes in TIGR is always equal to the air temperature at the lowest altitude in the temperature profile. Using the surface temperature as is to compute radiances is likely to produce artificially good retrievals near the surface if window channels are used. To avoid such misleading results the surface temperature was decorrelated from the temperature profile by adding to it a zero mean gaussian random variable with a standard deviation of 4 Kelvin.

In the simulations, brightness temperatures were computed at nineteen different channels. In addition to the MHS channels listed in Section 2., ten AMSU-A channels were simulated. Of these ten channels, which are listed in Table 4, the first two channels were only used for retrievals over ocean. For each channel the corresponding brightness temperature was obtained by averaging the brightnesses computed at the center frequencies of its sidebands and adding zero mean gaussian noise with standard deviation equal to the assumed sensitivity of the channel. The noise components at different frequencies were independent random variables.

To simulate brightness spectra observed from space using the radiative transfer model it is necessary to specify the emissivity of the surface over which the sensor is monitoring. In the simulations we considered two kinds of hypothetical surfaces as models for dry land and ocean. In both cases the surface was assumed to be flat. In the case of dry land the emissivity at each frequency was modeled as a random variable with mean of 90% and standard deviation of 5%. These random variables were 98% correlated among adjacent channels. Over ocean the emissivity was computed using a frequency and temperature dependent model for the dielectric constant of sea water [Kle77]. The salinity of water was set to thirty-five parts per thousand.

No.	Center Freq.(s) (MHz)	RMS Sensitivity (K)
1	23800	0.3
2	31400	0.3
3	50300	0.3
4	52800	0.3
5	53596 ± 115	0.3
6	54400	0.3
7	54940	0.3
8	55500	0.3
9	57290.344 = f_{LO}	0.3
10	f_{LO}± 217	0.3

Table 4: Additional channels used to perform the simulated water vapor retrievals.

B Cloud Liquid Water

At most of the frequencies of interest liquid water adds a non-negligible contribution to the radiance. It is therefore desirable to include the effect of clouds liquid water in the simulations to obtain more realistic retrieval accuracy estimates. We considered only non-precipitating clouds.

Since the TIGR database does not have liquid water content information it was necessary to add clouds using a heuristic procedure. Clouds were added to a radiosonde at any altitudes where the relative humidity exceeded 90% – nearly half of the radiosondes in TIGR exceeded this threshold. A cloud was modeled as a layer of uniform liquid water density occupying all adjacent levels for which the humidity threshold was exceeded. For each cloud the density was chosen randomly from the distribution

$$\Pr(\mathrm{x} \le x_o) = \begin{cases} 0 & \text{if } x_o < 0, \\ c \ln \left| \frac{\sqrt{(x_o-a)^2+b^2}+x_o-a}{\sqrt{a^2+b^2}-a} \right| & \text{if } 0 \le x_o \le d, \\ 1 & \text{otherwise.} \end{cases}$$

where $a = 0.05$, $b = a\sqrt{5}/2$, $d = 1.6$ and $\Pr(\mathrm{x} \le d) = 1$. Figure 7 shows the distribution on the interval [0,1.6]. This distribution is consistent with non-precipitating cloud data published by Aufm Kampe and Weichmann. Absorption due to liquid water was computed using the model by Liebe *et al.* [Lie91].

Denote the clear-air brightness observed at frequency f by $T_B(f)$ and the corresponding brightness observed in the presence of clouds by $\tilde{T}_B(f)$. Table 5 lists estimates of the mean and standard deviation of the brightness perturbations $\Delta T_B(f) = \tilde{T}_B(f) - T_B(f)$ observed at nadir over ocean. The estimates were obtained by averaging over the TIGR data.

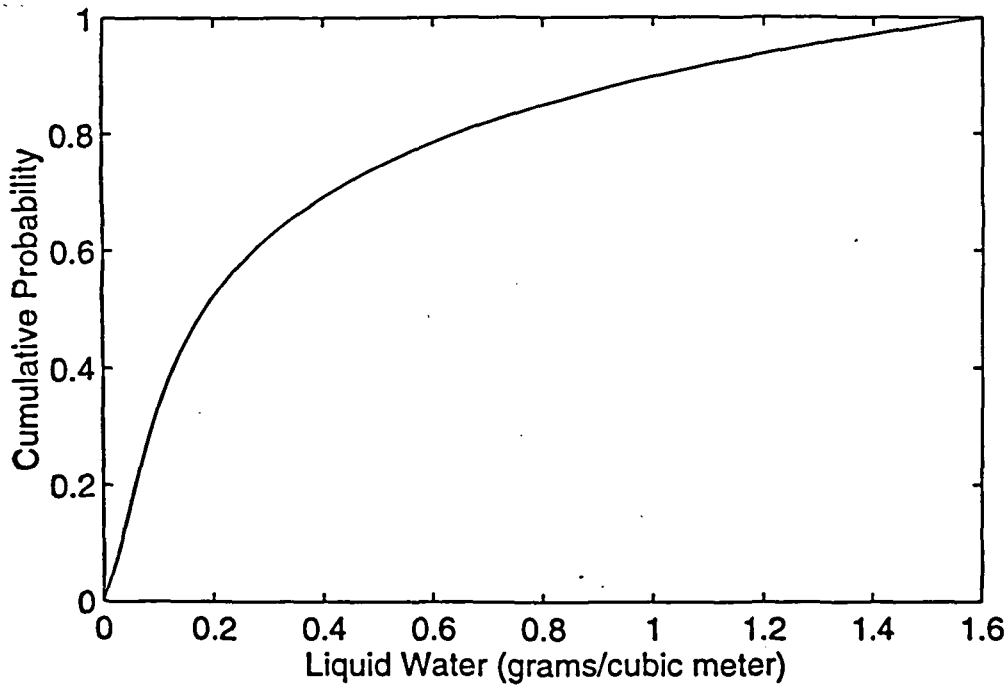

Figure 7: Cumulative probability distribution of the cloud liquid water density.

No.	Center Freq. (GHz)	Mean (K)	Std. Dev. (K)
1	23.8	6.0007	11.8272
2	31.4	8.6738	15.7725
3	50.3	4.2813	7.9418
4	52.8	-1.2796	5.1603
5	53.596 ± 0.115	-2.1129	5.2688
6	54.4	-1.5311	3.7183
7	54.94	-0.8937	2.3071
8	55.5	-0.3963	1.1436
9	57.290344	-0.0300	0.1274
10	57.290344 ± 0.217	-0.0052	0.0231
11	89.0	7.1081	13.0468
12	150.0	-1.1377	15.2023
13	183.31 ± 1.0	-6.6329	12.1235
14	183.31 ± 3.0	-8.8208	15.8554
15	183.31 ± 7.0	-8.9334	17.6628
16	183.31 ± 14.0	-6.5878	17.5359
17	118.75 ± 0.5	-0.9994	2.4685
18	118.75 ± 1.4	-4.5196	9.7222
19	118.75 ± 3.0	0.7444	11.9970

Table 5: Estimated mean and standard deviation of the brightness perturbations due to water clouds. The estimates were derived from nadiral brightness temperatures simulated over ocean using the TIGR data.

C Summary of Retrieval Errors

Sensor(s)	Angle	Pressure (mb)				
		200	307	525	800	955
MHS5	nadir	29.1	17.9	12.6	14.6	14.4
	50°	28.9	17.8	12.4	14.2	13.7
MHS7	nadir	20.3	15.8	11.6	13.4	13.6
	50°	20.4	16.0	11.5	13.4	13.4
MHS5 AMSU-A	nadir	14.5	15.1	10.6	11.4	10.7
	50°	14.2	14.7	10.4	11.3	10.6
MHS7 AMSU-A	nadir	14.4	15.0	10.6	11.4	11.1
	50°	14.0	14.7	10.8	11.2	10.9

Table 6: Clear-air retrieval accuracy over ocean. The errors are root-mean-square deviations in relative humidity (%).

Sensor(s)	Angle	Pressure (mb)				
		200	307	525	800	955
MHS5	nadir	22.8	18.3	16.3	16.4	14.2
	50°	24.3	17.8	16.3	16.8	14.2
MHS7	nadir	18.0	16.7	15.6	16.2	14.4
	50°	18.8	17.0	15.3	16.5	14.6
MHS5 AMSU-A	nadir	14.7	15.0	13.3	13.1	12.3
	50°	14.6	15.4	13.7	13.5	12.8
MHS7 AMSU-A	nadir	13.9	14.5	13.9	13.3	12.6
	50°	15.3	15.4	13.8	14.3	12.7

Table 7: Cloudy retrieval accuracy over ocean. The errors are root-mean-square deviations in relative humidity (%).

Sensor(s)	Angle	Pressure (mb)				
		200	307	525	800	955
MHS5 AMSU-A	nadir	14.4	15.4	11.5	16.7	16.1
MHS7 AMSU-A	nadir	14.9	15.4	11.6	16.9	16.0

Table 8: Clear-air retrieval accuracy over land. The errors are root-mean-square deviations in relative humidity (%).

Sensor(s)	Angle	Pressure (mb)				
		200	307	525	800	955
MHS5	50°	24.1	18.0	16.2	19.0	17.7
MHS7	50°	18.7	16.7	15.6	19.6	18.0

Table 9: Cloudy retrieval accuracy over land. The errors are root-mean-square deviations in relative humidity (%).

References

[Esc93] Escobar, J. *Base de Données pour la Restitution de Paramètres Atmosphériques à L'échelle Globale—Etude sur L'inversion per Réseaux de Neurones des Données des Sondeurs Verticaux Atmosphériques Satellitaires Présents et à venir*, Thesis, France: Ecole Polytechnique, 1993

[Kle77] Klein L., Swift, C. "An Improved Model for the Dielectric Constant of Sea Water at Microwave Frequencies." *IEEE Trans. Ant. and Prop.* **25** (1977):104–111

[Lie85] Liebe, H.J. "An Updated Model for Millimeter Wave Propagation in Moist Air." *Radio Science* **20** (1985):1069–1089

[Lie91] Liebe, H.J., Hufford, G.A., Manabe, T. "A Model for the Complex Permittivity of Water at Frequencies Below 1 THz." *Int. J. of IR and MM Waves.* **12** (1991):659–675

[Ros93] Rosenkranz, P.W. "Absorption of Microwaves by Atmospheric Gases." *Atmospheric Remote Sensing by Microwave Radiometry*, Janssen, M.A. (Ed.), New York:John Wiley & Sons, 1993

[Rum86] Rumelhart, D.E., Hinton, G., Williams, R. *Parallel Distributed Processing: Explorations in the Microstructure of Cognition. Vol. 1: Foundations*, Rumelhart, D.E. and McClelland, J.L. (Eds.), Massachusetts:MIT Press, 1986, 318–362

NASA

Report Documentation Page

1. Report No.	2. Government Accession No.	3. Recipient's Catalog No.

4. Title and Subtitle

Atmospheric Infrared Sounder

5. Report Date

August 22, 1995

6. Performing Organization Code

7. Author(s)

P. W. Rosenkranz and D. H. Staelin

8. Performing Organization Report No.

10. Work Unit No.

9. Performing Organization Name and Address

Massachusetts Institute of Technology
Research Laboratory of Electronics
Cambridge, MA 02139-4307

11. Contract or Grant No.

NAS5-31376

13. Type of Report and Period Covered

Semiannual
12/16/94 - 6/15/95

12. Sponsoring Agency Name and Address

NASA/Goddard Space Flight Center
Greenbelt, MD 20771

14. Sponsoring Agency Code

15. Supplementary Notes

16. Abstract

This report summarizes the activities of AIRS Team Members P.W. Rosenkranz and D.H. Staelin during the first half of 1995.

17. Key Words (Suggested by Author(s))	18. Distribution Statement		
AIRS, AMSU, MHS			
19. Security Classif. (of this report)	**20. Security Classif. (of this page)**	**21. No. of pages**	**22. Price**
Unclassified	Unclassified		